The Canadian Mineralogist
Vol. 33, pp. 889-905 (1995)

COORDINATION-GEOMETRY STRUCTURAL PATHWAYS IN Cu^{2+} OXYSALT MINERALS

PETER C. BURNS[1] AND FRANK C. HAWTHORNE

Department of Geological Sciences, University of Manitoba, Winnipeg, Manitoba R3T 2N2

ABSTRACT

Examination of available Cu^{2+} oxysalt mineral structures has shown that a number contain $Cu^{2+}\phi_n$ ($\phi = O^{2-}$, OH^-, H_2O; n = 4, 5, 6) coordination polyhedra that are transitional between the usual (4 + 2)-distorted octahedral, square-pyramidal, triangular-bipyramidal and square-planar geometries. The structural pathways between (4 + 2)-distorted octahedral and square-pyramidal, (4 + 2)-distorted octahedral and square-planar, and square-pyramidal and square-planar are represented in Cu^{2+} oxysalt minerals. Hartree–Fock molecular-orbital calculations for $(Cu^{2+}\phi_n)^{-n+2}$ model clusters using the STO–3G* basis-set were used to examine cluster geometries and the energetics of possible structural pathways. The calculations show the presence of a small energy-barrier along the pathway from (4 + 2)-distorted octahedral to square-planar, and a large energy-barrier along the pathway from (4 + 2)-distorted octahedral to triangular-bipyramidal. There are no energy-barriers along the other possible structural pathways between the normal coordination geometries. The results of these calculations are in good accord with $Cu^{2+}\phi_n$ geometries observed in minerals. This work shows that Cu^{2+} coordinations should be interpreted in terms of structural pathways between holosymmetric coordination-geometries.

Keywords: copper, copper oxysalt mineral, molecular orbital, Hartree–Fock, structural pathway, coordination geometry, theoretical mineralogy.

SOMMAIRE

Un examen de données structurales disponibles sur les oxysels de Cu^{2+} montre que certains de ces minéraux contiennent des polyèdres de coordinence $Cu^{2+}\phi_n$ (ϕ: O^{2-}, OH^-, H_2O; n = 4, 5, 6) qui sont géométriquement transitionnels entre l'octaèdre difforme (4 + 2), la pyramide carrée, la bipyramide triangulaire, et le plan carré. Les cheminements structuraux entre agencements octaédrique difforme (4 + 2) et pyramidal carré, entre agencements octaédrique difforme (4 + 2) et plan carré, et agencements pyramidal carré et plan carré seraient representés dans les oxysels de Cu^{2+}. Nos calculs d'orbites moléculaires selon la formule de Hartree–Fock pour les regroupements d'atomes $(Cu^{2+}\phi_n)^{-n+2}$, faisant appel au système d'orbites atomiques STO–3G*, ont été utilisés pour examiner les aspects géométriques des regroupements et pour en évaluer les aspects énergétiques dans le contexte de cheminements structuraux. Les résultats des calculs montrent la présence d'un faible seuil en énergie dans la transition menant d'octaèdre difforme (4 + 2) à plan carré, et d'un seuil plus important en énergie dans le cas de la transition menant d'octaèdre difforme (4 + 2) à agencement triangulaire bipyramidal. Par contre, il n'y a aucun seuil en énergie dans les cheminements structuraux entre les autres agencements géométries normaux. Ces résultats concordent bien avec les aspects géométriques des regroupements $Cu^{2+}\phi_n$ que nous trouvons dans les minéraux. Ce travail montre que la coordinence du Cu^{2+} peut s'interpréter en termes de cheminements structuraux entre agencements géométriques holosymétriques du polyèdre de coordinence.

(Traduit par la Rédaction)

Mots-clés: cuivre, oxysels de cuivre, orbites moléculaires, Hartree–Fock, cheminement structural, géometrie du polyèdre de coordinence, mineralogie théorique.

INTRODUCTION

There have been over two hundred and thirty Cu^{2+} oxysalt, oxide and hydroxide minerals (hereafter referred to as Cu^{2+} oxysalt minerals) described to date, and the crystal-structure arrangements are currently known for slightly less than half of these. Cu^{2+} oxysalt minerals show a myriad of structural varieties that in many instances are not isostructural with non-Cu^{2+} oxysalt analogues. The range of structure types is largely a result of the diversity of coordination polyhedra associated with the Cu^{2+} cation. Divalent copper commonly occurs in six-coordinated octahedral and trigonal-prismatic, five-coordinated square-pyramidal and triangular-bipyramidal, and four-coordinated square-planar geometries. Furthermore, by far the most

[1] Current address: Department of Earth and Planetary Sciences, University of New Mexico, Albuquerque, New Mexico 87131-1116, U.S.A.

common geometry of the coordination polyhedron is octahedral, which almost invariably involves a very strong distortion away from holosymmetric octahedral symmetry, to the extent that it is commonly difficult to decide on the most appropriate way of describing the coordination.

The highly distorted $Cu^{2+}\phi_6$ (ϕ: O^{2-}, OH^-, H_2O) octahedra in minerals are due to the electronic instability of the d^9 configuration of Cu^{2+} in an octahedral ligand-field (Fig. 1), as indicated by the Jahn–Teller theorem (Jahn & Teller 1937). Octahedral complexes with an electronic degeneracy in the e_g orbitals, as is the case for $Cu^{2+}\phi_6$, have a single Jahn–Teller-active normal mode of vibration of e_g symmetry (Deeth & Hitchman 1986). The instability of the $Cu^{2+}\phi_6$ octahedron is caused by vibronic couplings, but the Jahn–Teller stabilization energy ($\frac{1}{2}\Delta_{J-T}$, Fig. 1) is much greater than the energy of the e_g active mode of vibration, thus an essentially stationary state occurs.

The driving force of the Jahn–Teller distortion of $Cu^{2+}\phi_6$ octahedra is due to the unequal occupancies of the two e_g orbitals (Fig. 1), which are split by the distortion. Where the Jahn–Teller distortion occurs, the singly occupied orbital is destabilized by the same energy as the doubly occupied orbital is stabilized, resulting in a net energy stabilization. Ligand-field arguments (Orgel 1966) show that single occupancy of the dz^2 and dx^2–y^2 orbitals of Cu^{2+} will result in compressed (2 + 4) and elongated (4 + 2) $Cu^{2+}\phi_6$ octahedra, respectively. Although the (4 + 2)-distorted configuration is almost invariably adopted by $Cu^{2+}\phi_6$ octahedra in solids, the Jahn–Teller theorem (to first-order) does not indicate which of the two distortion geometries will be favored. However, arguments have been advanced to show that the second-order Jahn–Teller mixing of 3*d* and 4*s* orbitals on Cu^{2+} does favor the (4 + 2)-distorted $Cu^{2+}\phi_6$ octahedral configuration (Burdett 1980).

The $Cu^{2+}\phi_n$ (n = 4, 5 or 6) coordination geometries observed in a number of Cu^{2+} oxysalt minerals are significantly distorted from the principal ideal types [*i.e.*, (4 + 2)-distorted octahedral, square-pyramidal, triangular-bipyramidal and square-planar]. These geometries may be considered as intermediate between the different regular geometries of the coordination polyhedron, and may define structural pathways between the different (ideal) arrangements in coordination. The concept of structural pathways in Cu^{2+}-bearing inorganic compounds has been discussed previously (Hathaway 1984), but has not been applied specifically to minerals. Here, we combine a study of $Cu^{2+}\phi_n$ geometries in minerals and theoretical calculations to investigate the details and extent of these structural pathways.

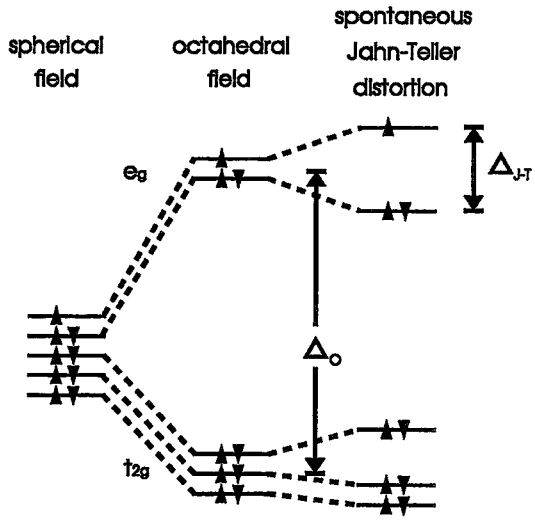

FIG. 1. The electronic energy-levels for Cu^{2+} in a spherical field (left), an octahedral field (middle), and a distorted octahedral field (right).

STRUCTURAL PATHWAYS IN Cu^{2+} OXYSALT MINERALS

Structural data for about 100 refined Cu^{2+} oxysalt minerals have been examined to determine which specific structural pathways are represented. The different possible pathways are shown in Figure 2, and each is considered explicitly below.

(4 + 2)-distorted octahedral ↔ square-pyramidal geometry

The most common Cu^{2+} coordination geometry observed is (4 + 2)-distorted octahedral. Square-pyramidal geometry may be derived from (4 + 2)-distorted octahedral geometry by removing one of the apical ligands, and moving the Cu^{2+} cation to above the equatorial plane in the direction of the remaining apical ligand (Fig. 3a). This pathway intrinsically contains (4 + 1 + 1)-distorted octahedral geometries, such that there are four short Cu–ϕ_{eq} bonds, one long Cu–ϕ_{ap} bond and one very long Cu-ϕ apical bond (Fig. 3a).

The division between (4 + 2)-distorted and (4 + 1 + 1)-distorted octahedral geometries is taken as the (arbitrary) point at which one Cu-ϕ_{ap} bond is 12.5% longer than the other. With this criterion, there are numerous (4 + 1 + 1)-distorted octahedra in Cu^{2+} oxysalt minerals (Table 1). *There is a continuous series of $Cu^{2+}\phi_6$ geometries between (4 + 2)-distorted octahedral and square-pyramidal*, and the (4 + 2)-distorted octahedral to square-pyramidal structural pathway is well represented in Cu^{2+} oxysalt minerals.

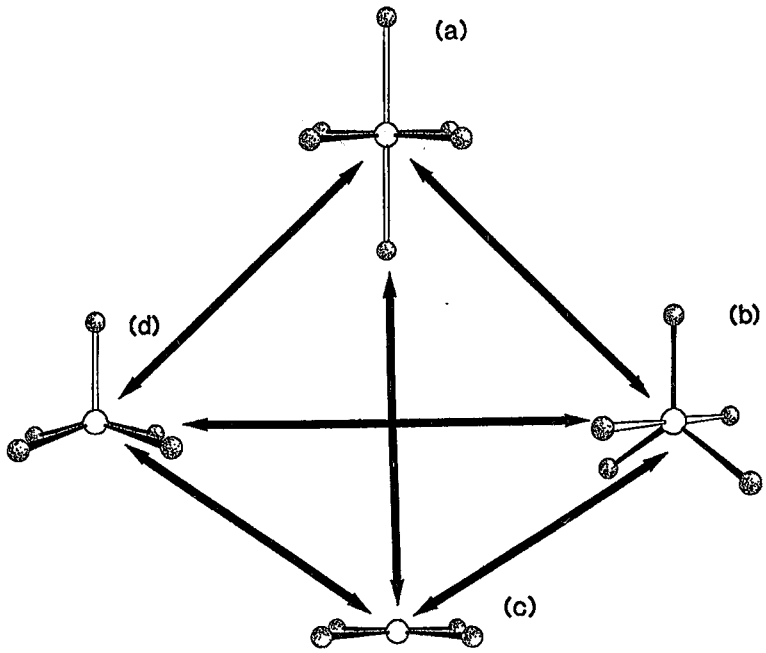

FIG. 2. Possible structural pathways in Cu^{2+} oxysalt minerals: (a) (4 + 2)-distorted octahedral; (b) triangular-bipyramidal; (c) square-planar; (d) square-pyramidal.

TABLE 1. Cu-ϕ BOND-LENGTHS (Å) IN Cu^{2+} OXYSALT MINERALS CONTAINING (4+1+1)-DISTORTED $Cu^{2+}\phi_6$ OCTAHEDRA

Mineral	Site	Cu-O_{eq}		Cu^{2+}-O_{ap}		Ref.
Lammerite	Cu(2)	1.941	1.947	2.282	2.782	1
		1.972	2.028			
Euchroite	Cu(2)	1.922	1.956	2.394	2.794	2
		1.983	2.004			
Cornetite	Cu(1)	1.923	1.940	2.470	3.087	3
		1.984	1.996			
	Cu(3)	1.925	1.930	2.280	2.821	
		1.988	2.023			
Plancheite	Cu(2)	1.934	1.975	2.310	2.617	4
		2.017	2.054			
Likasite	Cu(2)	1.96	1.96	2.42	2.83	5
		1.98	1.98			
Agardite	Cu	1.908	1.924	2.321	3.14	6
		1.991	2.011			
Kipushite	Cu(1)	1.97	1.97	2.24	2.94	7
		1.98	2.03			
	Cu(2)	1.99	1.99	2.15	2.73	
		2.03	2.05			
Clinoclase	Cu(1)	1.895	1.938	2.332	2.871	8
		1.992	2.074			
	Cu(2)	1.905	1.907	2.519	3.321	
		1.956	2.016			
	Cu(3)	1.916	1.976	2.272	2.995	
		2.000	2.033			
Wroewolfeite	Cu(3)	1.92	1.92	2.31	2.72	9
		1.98	2.01			
Posnjakite	Cu(2)	1.95	1.97	2.28	2.95	10
		1.99	2.01			
	Cu(4)	1.91	1.96	2.31	2.75	
		1.97	2.01			
Pseudo-malachite	Cu(2)	1.939	1.958	2.395	2.755	11
		1.974	1.985			
Spertiniite	Cu	1.948	1.948	2.356	2.915	12
		1.972	1.972			
Azurite	Cu(2)	1.938	1.943	2.358	2.761	13
		1.965	1.990			
Papagoite	Cu	1.936	1.936	2.402	3.016	14
		1.964	1.964			

References 1: Hawthorne (1986); 2: Eby & Hawthorne (1989a); 3: Eby & Hawthorne (1989b); 4: Evans & Mrose (1977); 5: Effenberger (1986); 6: Aruga & Nakai (1985); 7: Piret *et al.* (1985); 8: Eby & Hawthorne (1990); 9: Hawthorne & Groat (1985); 10: Mellini & Merlino (1979); 11: Shoemaker *et al.* (1977); 12: Oswald *et al.* (1990); 13: Zigan & Schuster (1972); 14: Groat & Hawthorne (1987)

(4 + 2)-distorted octahedral ↔ triangular-bipyramidal geometry

Ideally, the $Cu^{2+}\phi_5$ triangular-bipyramid may be derived from a (4 + 2)-distorted $Cu^{2+}\phi_6$ octahedron by removing one equatorial ligand and allowing the three remaining ligands to move to the corners of an equilateral triangle centered on the Cu^{2+} cation (Fig. 3b). This is a potential structural pathway that includes (3 + 1 + 2)-distorted, (3 + 3)-distorted and (3 + 2 + 1)-distorted octahedral geometries. There are no examples of these geometries in Cu^{2+} oxysalt minerals, and this structural pathway is not represented.

(4 + 2)-distorted octahedral ↔ square-planar geometry

Square-planar geometry is relatively rare in Cu^{2+} oxysalt minerals, but there are a few examples (Eby & Hawthorne 1993). Square-planar geometry may be derived from (4 + 2)-distorted octahedral geometry by removing both of the apical ligands (Fig. 3c). The structural pathway between (4 + 2)-distorted octahedral and square-planar geometries includes (4 + 2)-distorted octahedral geometries with two Cu–ϕ_{ap} bonds that are longer than the normal Cu–ϕ_{ap} bond-length observed in (4 + 2)-distorted octahedra (*i.e.*, ~2.4 – 2.5 Å). A number of Cu^{2+} oxysalt minerals contain such octahedra, which *are members of a structural pathway between (4 + 2)-distorted octahedral and square-planar geometries*. Examples with Cu–ϕ_{ap} greater than 2.70 Å are given in Table 2.

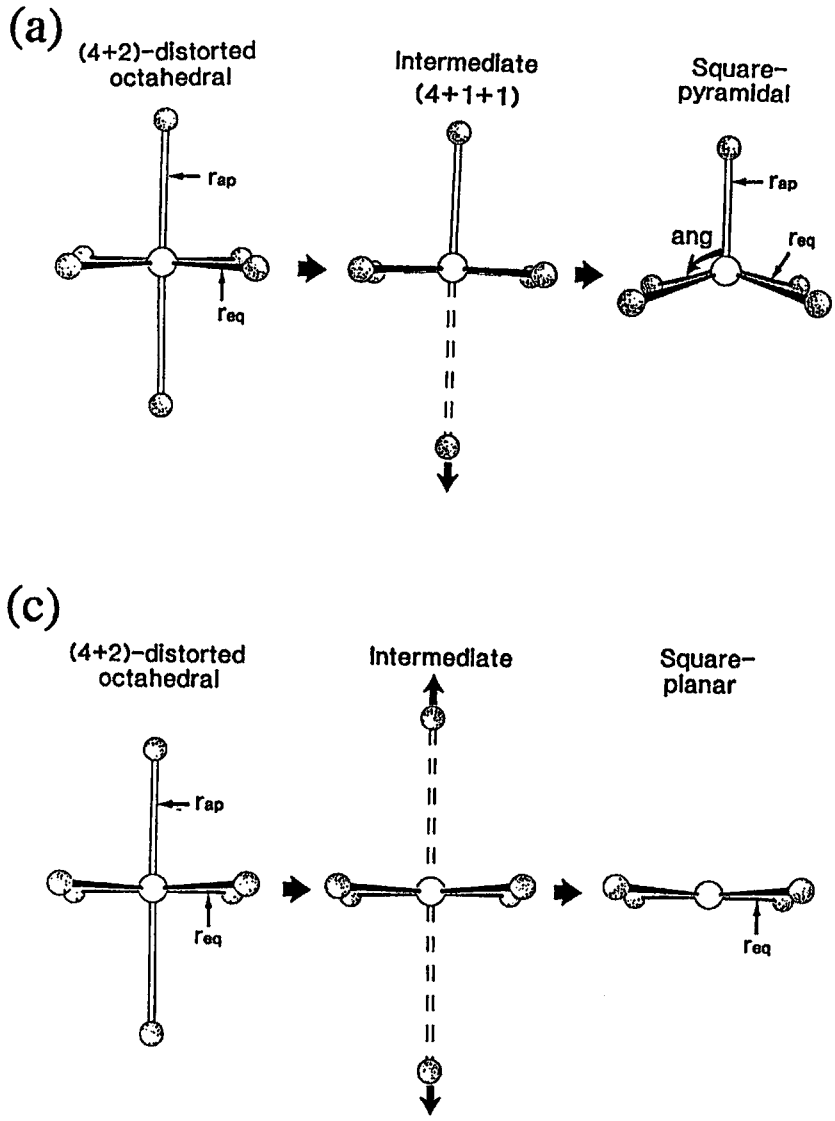

FIG. 3. Possible structural pathways in Cu^{2+} oxysalt minerals. The copper atoms are given as open circles, and oxygen atoms are shaded with a random-dot pattern: (a) (4 + 2)-distorted octahedral to square-pyramidal; (b) (4 + 2)-distorted octahedral to triangular-bipyramidal; (c) (4 + 2)-distorted octahedral to square-planar;

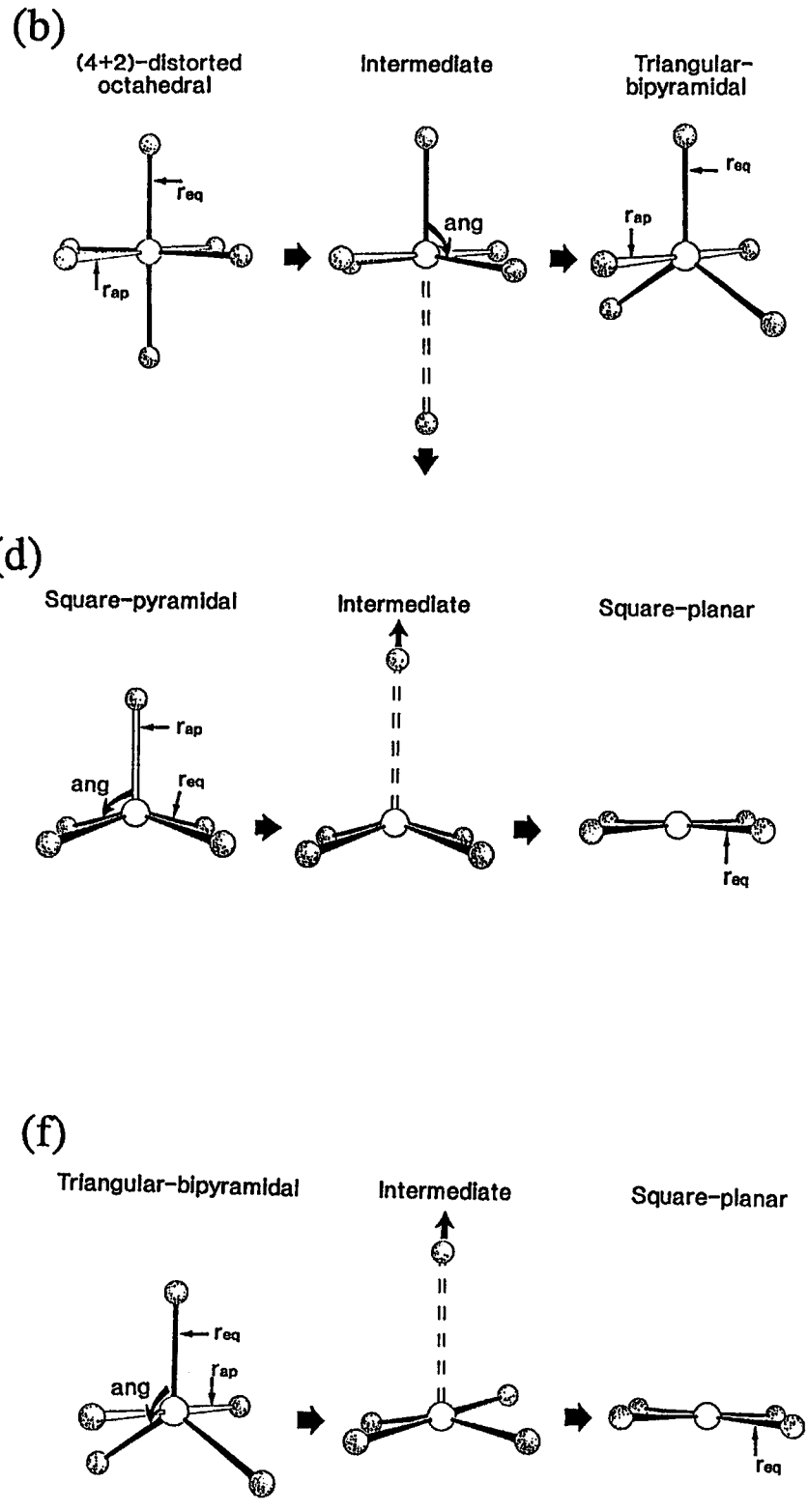

(d) square-pyramidal to square-planar; (e) square-pyramidal to triangular-bipyramidal; (f) triangular-bipyramidal to square-planar.

TABLE 2 Cu-ϕ BOND-LENGTHS (Å) IN EXAMPLES OF COORDINATION GEOMETRIES INTERMEDIATE BETWEEN (4+2)-DISTORTED OCTAHEDRAL AND SQUARE-PLANAR

Mineral	Site	r_{eq}		r_{ap}	Ref.
Lammerite	Cu(1)	1.933	1.933	2.923	1
		1.974	1.974	2.923	
Likasite	Cu(3)	1.96	1.96	2.83	2
		1.93	1.93	2.83	
Stringhamite	Cu(1)	1.918	1.972	3.383	3
		1.918	1.972	3.383	
	Cu(2)	1.934	1.934	3.053	
		1.960	1.960	3.053	
Azurite	Cu(1)	1.930	1.930	2.983	4
		1.946	1.946	3.323	
Hemmilite	Cu	1.939	1.939	3.067	5
		1.949	1.949	3.067	
Buttenbachite	Cu(1)	1.967	1.967	2.732	6
		1.967	1.967	2.732	
Stranskiite	Cu	1.907	1.907	3.134	7
		2.005	2.005	3.134	

References 1: Hawthorne (1986); 2: Effenberger (1986); 3: Hawthorne (1985); 4: Zigan & Schuster (1972); 5: Nakai (1986); 6: Fanfani *et al.* (1973); 7: Keller *et al.* (1979).

Square-pyramidal ↔ square-planar geometry

Removal of the apical ligand from an elongate square-pyramid allows the remaining atoms to rearrange into a square-planar geometry (Fig. 3d). Both of these geometries are fairly unusual in Cu^{2+} oxysalt minerals, but $Cu^{2+}\phi_5$ square-pyramids show a considerable range of Cu–ϕ_{ap} bond-length (Table 3: 2.24 to 2.52 Å), indicating that *the structural pathway from square-pyramidal to square-planar is represented in Cu^{2+} oxysalt minerals.*

Square-pyramidal ↔ triangular-bipyramidal geometry

The elongate square-pyramid may be derived from the compressed triangular-bipyramid by ϕ–Cu–ϕ adjustments and by small changes in Cu–ϕ bond-lengths (Fig. 3e). Owing to the simple structural pathway between these two coordination geometries, examples of intermediates are expected in minerals. However, Eby & Hawthorne (1990) did not find the complete range of transitional intermediates in Cu^{2+} oxysalt minerals, although they do occur in synthetic compounds (Effenberger 1988).

Triangular-bipyramidal ↔ square-planar geometry

Removal of an equatorial ligand from the triangular-bipyramid allows the remaining $Cu^{2+}\phi_4$ group to rearrange into square-planar geometry (Fig. 3f). Examination of $Cu^{2+}\phi_5$ triangular-bipyramids in Cu^{2+} oxysalt minerals (Table 3) shows that there is a considerable range of Cu–ϕ_{eq} bond-lengths, and there are examples (*i.e.*, stoiberite) that have one Cu–ϕ_{eq} bond considerably longer than the other two bonds. These triangular-bipyramids *may* belong to a triangular-bipyramidal to square-planar structural pathway, but there are too few examples to be conclusive.

TABLE 3. Cu^{2+} OXYSALT MINERALS WITH ($Cu^{2+}\phi_5$) POLYHEDRA

Square-Pyramidal

Mineral	Site	Cu-ϕ_{eq} (Å)		Cu-ϕ_{ap} (Å)	Ref.
Clinoclase	Cu(2)	1.905	1.956	2.519	1
		1.907	2.016		
	Cu(3)	1.916	2.000	2.275	
		1.976	2.033		
Litidionite	Cu	1.931	1.944	2.265	2
		1.948	1.953		
Callaghanite	Cu	1.926	1.959	2.483	3
		1.934	1.957		
Kinoite	Cu(1)	1.942	1.944	2.453	4
		1.942	1.944		
	Cu(2)	1.959	1.968	2.240	
		1.959	1.968		
Teinite	Cu	1.926	1.961	2.347	5
		1.953	1.967		
Ziesite	Cu	1.931	1.953	2.265	6
		1.948	1.950		
Blossite	Cu	1.880	1.955	2.542	7
		1.943	1.972		
Balyakinite	Cu	1.94	1.97	2.38	8
		1.97	1.98		
Chalcomenite	Cu	1.934	1.965	2.333	9
		1.955	1.986		
Fedotovite	Cu(1)	1.918	1.973	2.198	10
		1.963	2.026		
	Cu(2)	1.912	1.978	2.333	
		1.928	2.036		

Triangular-Bipyramidal

Mineral	Site	Cu-ϕ_{ap} (Å)	Cu-ϕ_{eq} (Å)		Ref.
Stoiberite	Cu(3)	1.932	1.969	2.287	11
		1.924	2.034		
	Cu(5)	1.890	1.964	2.230	
		1.930	2.034		
Dolerophanite	Cu(2)	1.906	2.155	2.155	12
		1.907	2.000		
Fingerite	Cu(6)	1.929	1.971	2.102	13
		1.907	2.147		
Olivenite	Cu(1)	1.92	1.99	2.05	14
		1.98	2.16		
Libethenite	Cu(2)	1.927	2.041	2.053	15
		1.939	2.053		
Mcbirneyite	Cu(2)	1.914	2.014	2.097	16
		1.923	2.124		

References 1: Eby & Hawthorne (1990); 2: Pozas *et al.* (1975); 3: Brunton (1973); 4: Laughon (1971); 5: Effenberger (1977); 6: Hughes & Brown (1988); 7: Calvo & Faggiani (1975); 8: Lindquist (1972); 9: Pasero & Perchiazzi (1989); 10: Starova *et al.* (1991); 11: Shannon & Calvo (1973); 12: Effenberger (1985); 13: Hughes & Hadidiacos (1985); 14: Toman (1977); 15: Cordsen (1978); 16: Shannon & Calvo (1972).

MOLECULAR-ORBITAL CALCULATIONS

Molecular-orbital (MO) calculations have been in use for about three decades, primarily to predict

geometries, energetics and stabilities of molecules. Molecular-orbital methods are based upon quantum mechanics, and range from empirical methods, which include an experimentally determined component, to *ab initio* methods, which include no experimentally determined parameters (apart from "universal" constants).

MO methods have been applied to relatively small molecules with considerable success, but it is only recently that computational sophistication and power have reached levels that allow application of these methods to minerals. At present, MO methods are being applied extensively to the study of properties of minerals with closed-shell molecular wavefunctions. Large-scale *ab initio* MO calculations that include entire crystal structures (with appropriate boundary conditions) are at present restricted to a small number of simple minerals.

As crystal MO calculations can only be done for a few minerals at today's level of computational power, there have been a considerable number of calculations done for molecular clusters of varying size as an approximation of local conditions in a crystal structure (*i.e.*, McCammon *et al.* 1991, Lasaga & Gibbs 1987, 1988, 1990, 1991, Gibbs 1982, Newton & Gibbs 1980). These cluster calculations are, at best, only an approximation of the local environment in a structure; there are long-range effects in periodic structures that are ignored by such calculations. Nevertheless, this type of calculation has proven to be of considerable value in the interpretation of structural variations in minerals. Here we present a brief review of the molecular-orbital method as it has been applied in this study. A more complete treatment may be found in Hehre *et al.* (1986).

Molecular-orbital methods

The *ab initio* MO method is an approximate method of describing electron distribution and motion. Individual electrons are assigned to one-electron functions referred to as *spin orbitals*, which are a product of spatial functions known as *molecular orbitals*, $\psi_1(x,y,z,)$, $\psi_2(x,y,z)$, $\psi_3(x,y,z)$..... and either α or β *spin-components*. These orbitals are used to form the *many-electron wavefunction*, a MO approximation of the solution to the Schrödinger equation.

Molecular orbitals commonly are constructed as linear combinations of N (known) *one-electron functions* Ω_u:

$$\psi_i = \Sigma c_{ui} \Omega_u \quad (1)$$

The functions Ω_u are *basis functions*, the collection of which constitutes the *basis set*. In many instances, basis functions are *atomic orbitals* for the atoms constituting the molecule; this is the *Linear Combination of Atomic Orbitals* (LCAO) approximation.

The Born–Oppenheimer approximation

The *Born–Oppenheimer* approximation assumes that the electronic terms of the molecular Hamiltonian operator are separable from the nuclear terms when the nuclear positions are held fixed. The Schrödinger time-independent non-relativistic equation is solved for all electrons in the system:

$$\hat{H}\psi^{elec} = E\psi^{elec} \quad (2)$$

where $\hat{H}$ is the electronic Hamiltonian differential operator that represents the total energy (potential and kinetic) of the system, and ψ^{elec} is the electronic wavefunction. The solutions of Equation 2 are known as *eigenvalues*, E; they give the electronic energy of the system.

The Hartree–Fock method

The principal problem to be addressed is finding a suitable function for ψ^{elec}. In the *Hartree–Fock approximation*, the electronic wavefunction ψ^{elec} is an "antisymmetrized" product of the one-electron functions ψ_i. These molecular orbitals (ψ_i) are linear combinations of atomic orbitals ϕ_u:

$$\psi_i = \Sigma c_{ui} \phi_u \quad (3)$$

where c_{ui} are known as the *molecular-orbital expansion coefficients*, and are to be determined in the calculation. The atomic orbitals (ϕ_u) used in the calculation are referred to as the basis set; there are numerous basis sets available in the literature.

The Hartree–Fock wavefunction is a determinant constructed from molecular orbitals, which, in turn, may be expanded as a set of basis functions (ϕ_u). In Hartree–Fock theory, the optimal values of the expansion coefficients c_{ui} are determined using the variational theorem (Hehre *et al.* 1986), which indicates that for any antisymmetric normalized wavefunction ψ, the expectation energy (E′) may be obtained from the integral

$$E' = \int \psi^* \hat{H} \psi \, d\tau \quad (4)$$

The expectation energy (E′) provides an upper bound to the correct energy (E) of the system. The molecular-orbital expansion coefficients c_{ui} are adjusted for a given basis-set by minimizing the expectation energy (E′) of the system:

$$\frac{\partial E'}{\partial c_{ui}} = 0 \text{ (all u,i)} \quad (5)$$

How close the Hartree–Fock energy is to the correct energy (within the limits of quantum mechanics) depends on the single-determinant wavefunction and the basis set used. As the size of the basis set is

increased for a given calculation, the energy obtained will converge to the minimum energy that may be obtained within the Hartree–Fock approximation (termed the Hartree–Fock limit). However, this energy will still be greater than the true energy of the system owing to the correlation of electrons, a feature that is largely ignored by the Hartree–Fock calculation.

The variation condition (equation 5) gives rise to a series of algebraic equations for c_{ui} that are collectively referred to as the Roothaan–Hall equations. These equations are not linear, thus their solution involves an iterative process known as self-consistent-field (SCF) calculations.

Selection of a basis set

The selection of the most appropriate basis set is the most important decision to be made when doing Hartree–Fock calculations, and the choice is complicated by the large number of basis sets available in the literature. When selecting basis sets for MO calculations, the desired accuracy is balanced against the cost of the calculations, as the computational expense of a Hartree–Fock MO calculation is proportional to the fourth power of the number of basis functions (Hehre *et al.* 1986).

The STO–3G* minimal basis set (Hehre *et al.* 1969, Collins *et al.* 1976) is perhaps the most widely used basis set. The STO–3G* basis set for first-row transition metals has been widely used for the calculation of molecular properties. Although it has shortcomings, some aspects of bonding, particularly in organometallic complexes, are well described (Dobbs & Hehre 1987). For example, Gibbs (1982) described the use of the STO–3G* basis set in the optimization of the geometry of 18 hydroxyacid molecules with [3]-, [4]- and [6]-coordinate first- and second-row ions. The calculated bond-lengths were found to differ on average by less than 0.04 Å from the mean observed bond-lengths. Pople (1976) reported that the mean absolute deviation from experiment for SCF STO–3G bond lengths in several dozen molecules containing H, C, N, O and F is 0.030 Å. More recently, McCammon *et al.* (1991) and Lasaga & Gibbs (1988) have used the STO–3G* minimal basis set to calculate physical properties of minerals. The main attraction of the STO–3G* basis set (other than the relatively low cost of the calculations) is its effectiveness in predicting geometries.

Ab Initio Hartree–Fock MO Examination of Structural Pathways between $Cu^{2+}\phi_n$ Coordination Geometries

Molecular-orbital calculations for $Cu^{2+}\phi_n$ clusters with geometries that map the structural pathways between various $Cu^{2+}\phi_n$ coordination geometries will provide both theoretical optimized geometries and energies along the structural pathways. The following Hartree–Fock calculations were done with Gaussian 86 (Frisch *et al.* 1984) and Gaussian 92 (Frisch *et al.* 1992). All calculations were UHF (spin–unrestricted open shell) and were done using the STO–3G* basis set (Hehre *et al.* 1969, Collins *et al.* 1976). No spin contamination was observed in the final wavefunctions. Where cluster geometries were optimized, atomic positions were adjusted until the maximum forces on any atom did not exceed 0.00045 Hartrees/Bohr and the maximum displacement of any atom in the previous cycle did not exceed 0.0009 Å; all Cu–O–H bond-angles were fixed at 110°, and H–O bond-lengths, at 0.98 Å (*cf.* Lasaga & Gibbs 1988).

Hartree–Fock calculations in some cases tend to give poor descriptions of systems where bond breaking occurs (Hehre *et al.* 1986). UHF (spin unrestricted) calculations perform better for such systems than do closed-shell calculations. However, the lack of a proper treatment of electron correlation, particularly of the bonding electrons, may result in poorly estimated energies. In order to test the validity of the Hartree–Fock calculations reported here for $Cu^{2+}\phi_n$ structural pathways, partial configuration interaction (CID) and Møler-Plesset (MP2 and MP3) calculations were done for a selection of points along some of the structural pathways. Although the absolute values of the energies are different, the electron-correlation calculations give similar trends (see below, Tables 6 and 7), and do not alter the conclusions drawn from the UHF calculations.

(4 + 2)-distorted octahedral ↔ square-pyramidal geometry

The starting point for examination of this pathway was the $[Cu^{2+}(OH)_6]^{4-}$ cluster [(4 + 2)-distorted octahedron] with optimized Cu-ϕ bond lengths. The

TABLE 4. REOPTIMIZED* $[Cu^{2+}(OH)_6]^{4-}$ CLUSTER GEOMETRIES ALONG THE STRUCTURAL PATHWAY FROM (4+2)-DISTORTED OCTAHEDRAL TO SQUARE-PYRAMIDAL

Step	r_{ap}(fixed) (Å)	r_{eq} (Å)	r_{ap} (Å)	ang (°)	Energy (Hartrees)
(4+2)-distorted Octahedron	2.427	2.081	2.427	90+	-2066.5750
1	2.50	2.076	2.401	90.41	-2066.5750
2	2.60	2.070	2.373	90.93	-2066.5749
3	2.70	2.063	2.350	91.42	-2066.5752
4	2.85	2.055	2.322	92.12	-2066.5769
5	3.00	2.047	2.298	92.76	-2066.5804
6	3.20	2.040	2.274	93.49	-2066.5880
7	3.50	2.033	2.248	94.37	-2066.6042
8	5.00	2.026	2.187	96.87	-2066.6935
9	7.00	2.027	2.155	98.52	-2066.7693
10	8.00	2.028	2.146	98.99	-2066.7947
Square Pyramidal		2.040	2.112	101.15	

* Refer to Figure 3a for an explanation of optimized parameters.
\+ Held fixed at 90° for the (4+2)-distorted octahedron optimization

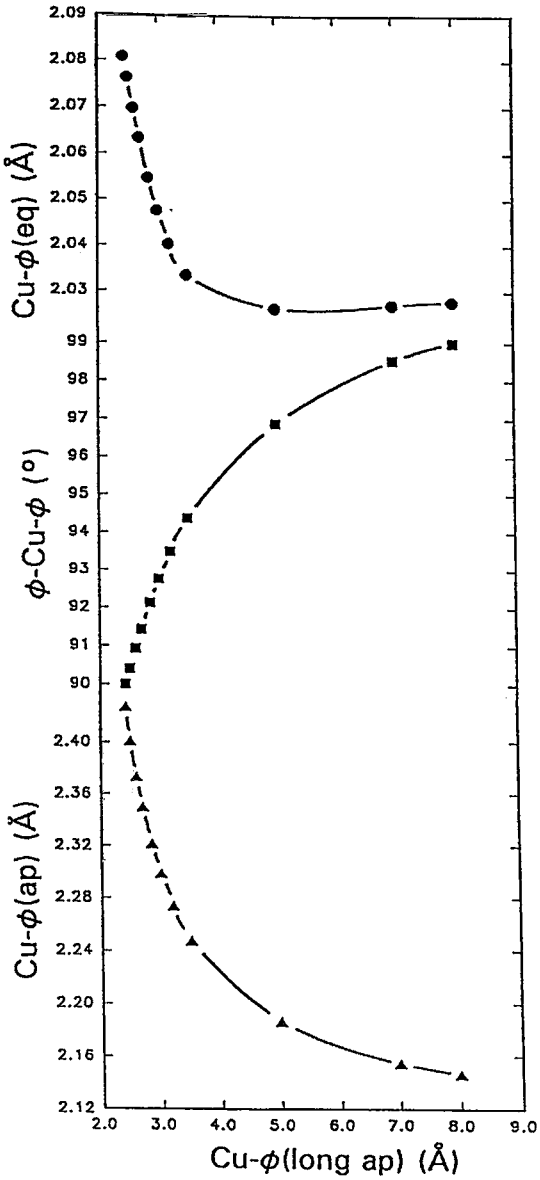

FIG. 4. Optimized geometries along the structural pathway from (4 + 2)-distorted octahedral to square-pyramidal.

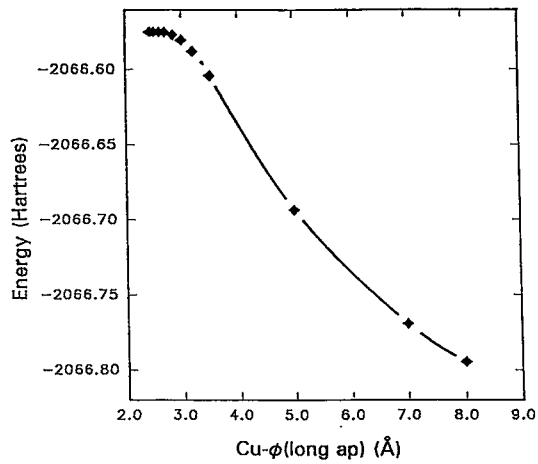

FIG. 5. Cluster energies along the structural pathway from (4 + 2)-distorted octahedral to square-pyramidal.

structural pathway was modeled by increasing one of the Cu-ϕ_{ap} bond lengths in a stepwise fashion, such that the apical ligand is moved away from the Cu^{2+} cation in a direction perpendicular to the equatorial plane (Fig. 3a). For each step, the Cu–ϕ_{ap} bond length was fixed, and the rest of the cluster geometry was reoptimized. Included in the reoptimization were the four Cu–ϕ_{eq} bond lengths (constrained to be equivalent), the remaining Cu–ϕ_{ap} bond length, and the four ϕ_{ap}–Cu–ϕ_{eq} angles (constrained to be equivalent) (labeled r_{eq}, r_{ap} and ang in Fig. 3a). The optimized geometries and cluster energies are given in Table 4 and Figures 4 and 5.

These calculations show that as the apical atom of oxygen moves away from its equilibrium position at 2.427 Å from the Cu^{2+} cation, the remaining atoms rapidly rearrange toward square-pyramidal geometry (Fig. 4). Most of the rearrangement occurs before the apical oxygen atom is 3.0 Å from the Cu^{2+} cation, and it is virtually complete before the oxygen atom is 3.5 Å from the Cu^{2+} cation. *There is no energy-barrier along this pathway* (Fig. 5). These results support the proposed structural pathway between (4 + 2)-distorted octahedral and square-pyramidal geometries in Cu^{2+} oxysalt minerals, as indicated by the presence of (4 + 1 + 1)-distorted octahedral geometries.

(4 + 2)-distorted octahedral ↔ triangular-bipyramidal geometry

The starting point for examination of the (4 + 2)-distorted octahedral to triangular-bipyramidal structural pathway was the $[Cu^{2+}(OH)_6]^{4-}$ cluster with optimized (4 + 2)-distorted octahedral Cu–ϕ bond-lengths. The structural pathway was modeled by extending one Cu–ϕ_{eq} bond in a stepwise fashion while reoptimizing the geometry of the remaining cluster. Included in the reoptimization were the other Cu–ϕ_{eq} bond lengths (constrained to be equivalent), the Cu–ϕ_{ap} bond lengths (constrained to be equivalent), and the ϕ_{eq}–Cu–ϕ_{eq} angles (labeled r_{eq}, r_{ap} and ang in Fig. 3b).

TABLE 5. REOPTIMIZED* $[Cu^{2+}(OH)_6]^{4+}$ CLUSTER GEOMETRIES ALONG THE STRUCTURAL PATHWAY FROM (4+2)-DISTORTED OCTAHEDRAL TO TRIANGULAR-BIPYRAMIDAL

Step	r_{eq}(fixed) (Å)	r_{eq} (Å)	r_{ap} (Å)	ang (°)	Energy (Hartrees)
(4+2)-distorted Octahedron	2.081	2.081	2.427	90*	-2066.5750
1	2.30	2.088	2.314	91.42	-2066.5704
2	2.50	2.065	2.189	91.84	-2066.5694
3	2.70	2.065	2.158	93.27	-2066.5671
4	2.90	2.060	2.136	94.75	-2066.5676
5	3.10	2.055	2.118	96.25	-2066.5718
Triangular Bipyramidal		2.079	2.017	120.0	

+ refer to Figure 3b for an explanation of optimized parameters
* Held fixed at 90° for the (4+2)-distorted octahedral optimization.

The optimized geometries and cluster energies are given in Table 5 and Figures 6 and 7.

As the Cu–ϕ_{eq} distance increases, the geometry of the remaining cluster distorts toward a triangular-bipyramidal arrangement (Fig. 6). However, this pathway has a steep energy-barrier (Fig. 7), which explains why the complete range of transitional geometries is not observed in Cu^{2+} oxysalt minerals.

(4 + 2)-distorted octahedral ↔ square-planar geometry

The starting point for examination of the structural pathway between (4 + 2)-distorted octahedral and square-planar geometries was the $[Cu^{2+}(OH)_6]^{4-}$ cluster with optimized bond-lengths in the (4 + 2)-distorted octahedron. The pathway was modeled by increasing both Cu–ϕ_{ap} bond lengths in a stepwise fashion and reoptimizing the Cu–ϕ_{eq} bond lengths for each step (Fig. 3c). The optimized geometries and cluster energies are given in Table 6 and in Figure 8.

The remaining atoms rearrange toward a square-planar geometry as the apical atoms of oxygen move away from the Cu^{2+} cation (Fig. 8). The majority of the transformation to the (contracted) square-planar arrangement occurs before Cu–ϕ_{ap} attains a value of 3.0 Å. The calculations indicate that there is a shallow energy-barrier along the structural pathway from (4 + 2)-distorted octahedra to square-planar geometry (Fig. 8), which reaches a maximum at about Cu–ϕ_{ap} = 2.70 Å, where the energy of the cluster is 0.0016 Hartrees (4.2 kJ/mole) greater than the energy of the (4 + 2)-distorted octahedron. However, it is apparent from observed $Cu^{2+}\phi_n$ geometries (Table 2) that this energy-barrier is not sufficiently steep to prevent the occurrence of this structural pathway in minerals. Also, this energy-barrier may be avoided (as shown above and below) by passing through a (4 + 1 + 1)-distorted intermediate geometry.

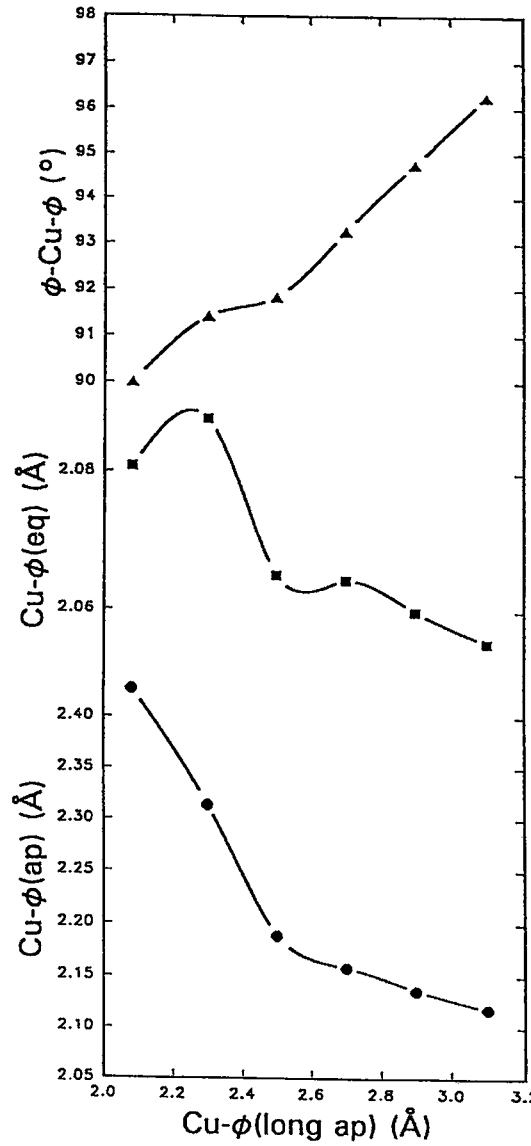

FIG. 6. Optimized geometries along the structural pathway from (4 + 2)-distorted octahedral to triangular-bipyramidal.

Square-pyramidal ↔ square-planar geometry

The starting point was the $[Cu^{2+}(OH)_5]^{3-}$ cluster with optimized square-pyramidal geometry. The pathway was modeled by extending the Cu–ϕ_{ap} bond length in a stepwise fashion and reoptimizing the geometry of the remaining cluster. The Cu–ϕ_{eq} bond

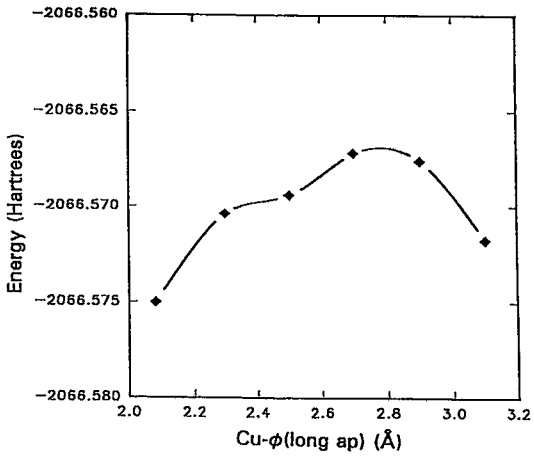

FIG. 7. Cluster energies along the structural pathway from (4 + 2)-distorted octahedral to triangular-bipyramidal.

lengths (constrained to be equivalent) and ϕ_{ap}–Cu–ϕ_{eq} angles (constrained to be equivalent) were included in the optimization (shown as r_{eq} and ang in Fig. 3d). The optimized geometries and cluster energies are given in Table 7 and Figure 9.

TABLE 6. REOPTIMIZED* $[Cu^{2+}(OH)_6]^{4-}$ CLUSTER GEOMETRIES ALONG THE STRUCTURAL PATHWAY FROM (4+2)-DISTORTED OCTAHEDRAL TO SQUARE-PLANAR

Step	r_{ap} (Å)	r_{eq}(optimized, Å)	Energy (Hartrees)
1	2.00	2.283	-2066.5234
2	2.10	2.164	-2066.5621
3	2.20	2.134	-2066.5699
4	2.30	2.109	-2066.5737
5	2.40	2.086	-2066.5750
(4+2)-Octahedron	2.427	2.081	-2066.5750
6	2.50	2.067	-2066.5748
7	2.60	2.050	-2066.5740
8	2.70	2.034	-2066.5735
9	2.80	2.021	-2066.5736
10	2.90	2.009	-2066.5748
11	3.00	1.999	-2066.5773
12	3.10	1.990	-2066.5812
13	3.20	1.983	-2066.5865
14	3.30	1.976	-2066.5931
15	3.40	1.971	-2066.6008
Square-planar		1.931	

Electron-Correlation Calculations

Step	E(UHF)	E(CID)	E(MP2)	E(MP3)
6	-2066.5748	-2066.9012	-2066.9028	-2066.9282
11	-2066.5773	-2066.9055	-2066.9104	-2066.9316
15	-2066.6008	-2066.9306	-2066.9373	-2066.9567

* Refer to Figure 3c for an explanation of the optimized parameters.

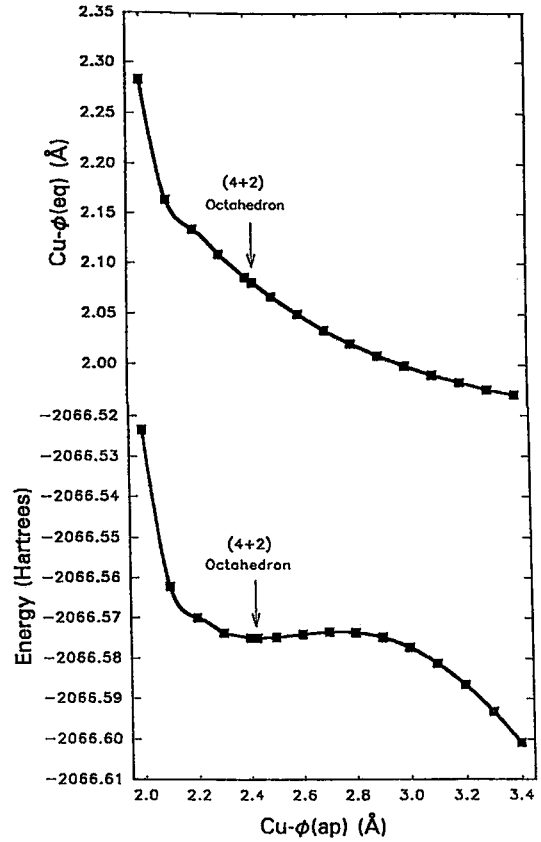

FIG. 8. Optimized geometries and cluster energies along the structural pathway from (4 + 2)-distorted octahedral to square-planar.

The remaining atoms gradually rearrange toward square-planar geometry while the apical ligand is removed (Fig. 9), and there is no energy-barrier along this structural pathway (Fig. 9). These calculations support the hypothesis that at least some of *the square-pyramidal geometries observed in Cu^{2+} oxysalt minerals belong to this structural pathway.*

Square-pyramidal ↔ triangular-bipyramidal geometry

This structural pathway was modeled using the optimized geometry for the $[Cu^{2+}(OH)_5]^{3-}$ cluster. Energies were calculated for nine equally spaced steps along the most direct geometrical pathway between the two coordination geometries (Table 8, Fig. 10). The calculated Hartree–Fock SCF energy for each step along the structural pathway shows that *there is no energy-barrier between the two $Cu^{2+}\phi_5$ geometries.* These calculations indicate that the structural pathway

TABLE 7. REOPTIMIZED+ $[Cu^{2+}(OH)_5]^{3-}$ CLUSTER GEOMETRIES ALONG THE STRUCTURAL PATHWAY FROM SQUARE-PYRAMIDAL TO SQUARE-PLANAR

Step	r_{ap}(fixed) (Å)	r_{eq} (Å)	ang (°)	Energy (Hartrees)
Square-Pyramidal	2.112	2.040	101.14	-1992.9160
1	2.20	2.033	100.79	-1992.9149
2	2.30	2.027	100.39	-1992.9115
3	2.40	2.021	99.99	-1992.9066
4	2.50	2.015	99.59	-1992.9009
5	2.60	2.009	99.19	-1992.8949
6	2.70	2.003	98.79	-1992.8891
7	2.80	1.998	98.38	-1992.8838
8	2.90	1.993	97.99	-1992.8792
9	3.00	1.988	97.61	-1992.8756
10	3.20	1.978	96.86	-1992.8715
11	3.40	1.973	96.23	-1992.8714
Square-Planar		1.931	90.00	

Electron-Correlation Calculations

Step	E(UHF)	E(CID)	E(MP2)	E(MP3)
1	-1992.9149	-1993.2292	-1993.2345	-1993.2528
7	-1992.8838	-1993.1976	-1993.2058	-1993.2211
11	-1992.8714	-1993.1835	-1993.1922	-1993.2056

+ Refer to Figure 8d for an explanation of the optimized parameters.

between square-pyramidal and triangular-bipyramidal may occur in minerals.

Triangular-bipyramidal ↔ square-planar geometry

The starting point was the $[Cu^{2+}(OH)_5]^{3-}$ cluster with optimized triangular-bipyramidal geometry. The pathway was modeled by extending one of the Cu–ϕ_{eq} bond lengths in a stepwise fashion and reoptimizing the geometry of the remaining cluster. The other Cu–ϕ_{eq} bond lengths (constrained to be equivalent), the Cu–ϕ_{ap} bond lengths (constrained to be equivalent) and the ϕ_{eq}–Cu–ϕ_{eq} bond angles (constrained to be equivalent) were included in the optimization (shown as r_{eq}, r_{ap} and ang in Fig. 3f). The optimized geometries and cluster energies are given in Table 9 and Figure 11.

The remaining cluster gradually distorts toward square-planar geometry as the equatorial ligand is removed (Fig. 11), and there is no energy-barrier along this pathway. Thus, the triangular-bipyramidal to square-planar structural pathway probably occurs in Cu^{2+} oxysalt minerals.

Discussion

Molecular-orbital calculations for $Cu^{2+}\phi_n$ polyhedra have given equilibrium geometries for isolated model clusters of atoms corresponding to (4 + 2)-distorted octahedral, square-pyramidal, triangular-bipyramidal

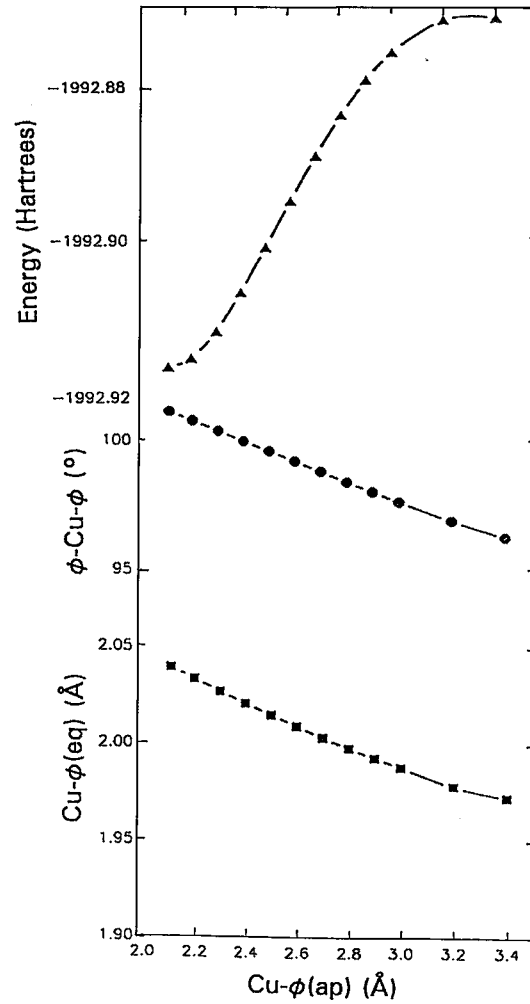

FIG. 9. Optimized geometries and cluster energies along the structural pathway from square-pyramidal to square-planar.

and square-planar arrangements. However, the geometries of such clusters of atoms embedded in a crystal structure are not necessarily identical to the equilibrium geometries of the isolated clusters, as the crystal-structure environment often exerts forces that lead to the deformation of the cluster (Bürgi & Dunitz 1983). This suggests that the comparison of the observed geometries of a specific cluster of atoms in many structures will provide information on the potential-energy surface of the cluster. The underlying assumption of the structure-correlation method (Bürgi & Dunitz 1983) is that the geometries of the cluster of atoms in the observed structures will tend to concentrate in low-lying regions of the potential-energy surface of the cluster. In the case of $Cu^{2+}\phi_n$ polyhedra

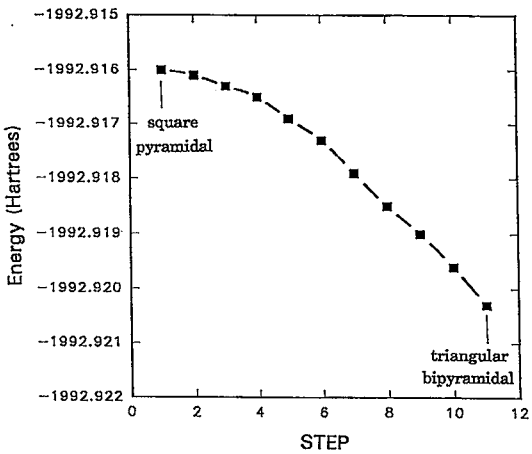

FIG. 10. Cluster energies for the transition from square-pyramidal to triangular-bipyramidal along the most direct geometric pathway.

in Cu^{2+} oxysalt minerals, the forces exerted upon the $Cu^{2+}\phi_n$ polyhedron by the remainder of the crystal structure commonly lead to a coordination geometry that is transitional between two of the principal types. In Cu^{2+} oxysalt minerals, $Cu^{2+}\phi_n$ coordination polyhedra transitional between (a) (4 + 2)-distorted octahedral and square-pyramidal, (b) (4 + 2)-distorted octahedral and square-planar, and (c) square-pyramidal and square-planar are quite common, and these intermediate $Cu^{2+}\phi_n$ geometries define coordination-geometry structural pathways between these principal coordination types. This implies that each of these structural pathways corresponds to a potential-surface energy valley between the principal coordination types,

TABLE 8. HARTREE-FOCK ENERGIES OF CLUSTER GEOMETRIES* TRANSITIONAL BETWEEN TRIANGULAR-BIPYRAMIDAL AND SQUARE-PYRAMIDAL COORDINATION

Step	Cu-O1 (Å)	Cu-O2 (Å)	Cu-O3 (Å)	α_1(°)	α_2(°)	Energy (Hartrees)
Triangular Bipyramid	2.079	2.017	2.079	90	120	-1992.9203
1	2.082	2.019	2.075	91.11	118.11	-1992.9196
2	2.086	2.021	2.071	92.23	116.23	-1992.9190
3	2.089	2.024	2.067	93.34	114.34	-1992.9185
4	2.092	2.026	2.063	94.46	112.46	-1992.9179
5	2.096	2.028	2.059	95.57	110.57	-1992.9173
6	2.099	2.030	2.055	96.68	108.68	-1992.9169
7	2.102	2.033	2.051	97.80	106.80	-1992.9165
8	2.106	2.035	2.047	98.91	104.91	-1992.9163
9	2.109	2.037	2.044	100.03	103.03	-1992.9161
Square Pyramid	2.112	2.040	2.040	101.14	101.14	-1992.9160

* Fig. 3e gives the structural pathway geometries used for these calculations

TABLE 9. REOPTIMIZED $[Cu^{2+}(OH)_6]^{3+}$ CLUSTER GEOMETRIES ALONG THE STRUCTURAL PATHWAY FROM TRIANGULAR-BIPYRAMIDAL TO SQUARE-PLANAR

Step	r_{eq}(fixed) (Å)	r_{eq}(Å)	r_{ap}(Å)	ang(°)	Energy (Hartrees)
Triangular bipyramidal	2.079	2.079	2.017	120	-1992.9203
1	2.30	2.066	2.000	118.34	-1992.9134
2	2.40	2.056	1.996	116.13	-1992.9077
3	2.50	2.046	1.993	114.20	-1992.9014
4	2.60	2.039	1.988	112.62	-1992.8948
5	2.70	2.030	1.985	111.37	-1992.8885
6	2.80	2.023	1.980	110.12	-1992.8827
7	2.90	2.016	1.976	109.10	-1992.8776
8	3.00	2.011	1.973	108.26	-1992.8735
9	3.25	1.998	1.965	106.09	-1992.8678
10	3.50	1.987	1.959	104.52	-1992.8684
Square planar		1.931	1.931	90	

+ Refer to Figure 3f for an explanation of the optimized parameters

and the MO calculations reported here have demonstrated that such an energy valley exists in each case.

Molecular-orbital calculations for model clusters of atoms have given geometries and energetics of $Cu^{2+}\phi_n$ coordination geometries transitional between the principal types. A summary of the MO investigations of $Cu^{2+}\phi_n$ coordination-geometry structural pathways is given in Figure 12, where arrows indicate continuous pathways, as indicated by the calculations, and broken lines denote energy-barriers. The calculations indicate that there is a significant energy-barrier along the structural pathway from (4 + 2)-distorted octahedral to triangular-bipyramidal geometry, and this structural pathway is not represented in minerals. The calculations also indicate that there is a small energy-barrier along the structural pathway between (4 + 2)-distorted octahedral and square-planar geometry, but an almost continuous series of $Cu^{2+}\phi_n$ coordination geometries corresponding to this structural pathway occurs in minerals, indicating that the small energy-barrier is overridden by local structural effects. Also, the calculations indicate that this energy-barrier may be avoided if the pathway followed is (4 + 2)-distorted octahedral to (4 + 1 + 1)-distorted octahedral to square-planar geometry.

The MO calculations reported here indicate that there is no energy-barrier between square-pyramidal and triangular-bipyramidal $Cu^{2+}\phi_5$ geometries. It remains unclear as to why representative geometries of the square-pyramidal to triangular-bipyramidal structural pathway have not been observed in Cu^{2+} oxysalt minerals; this is probably due to the relatively small number of examples of these coordination geometries found so far, as there is a complete range in synthetic compounds. There are apparently no intrinsic restrictions from the topological or energetic aspects of the overall structural arrangements.

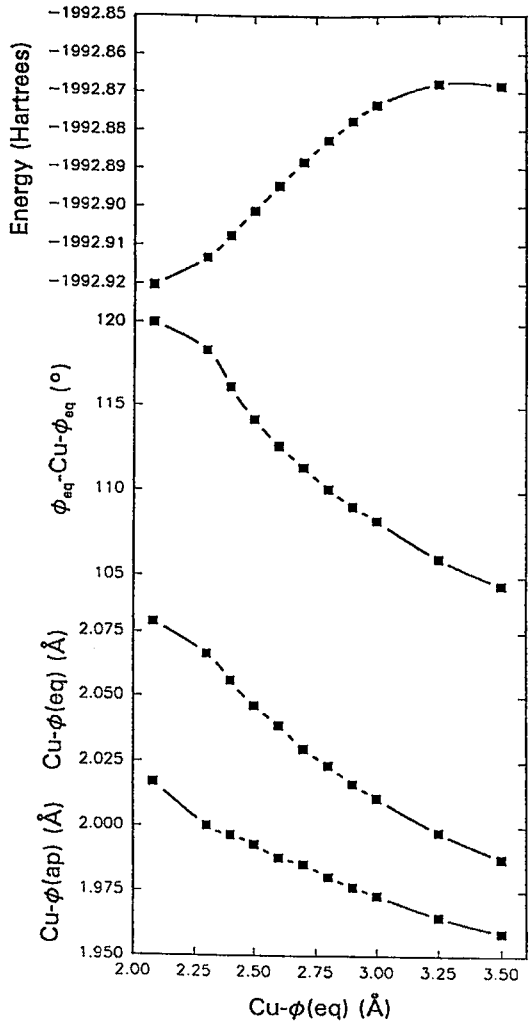

FIG. 11. Optimized geometries and cluster energies along the structural pathway from triangular-bipyramidal to square-planar.

It is now apparent that many Cu^{2+} oxysalt minerals contain $Cu^{2+}\phi_n$ coordination polyhedra that are members of one of the structural pathways shown in Figure 12, rather than one of the principal coordination types. In past studies of Cu^{2+} oxysalt minerals, these structural pathways have not been recognized, and confusion has often arisen concerning these intermediate coordination geometries. This work indicates that Cu^{2+} coordination geometries should be described out to perhaps 3.2 Å (without necessarily implying that a specific long interaction is significant), and interpreted in terms of the concept of structural pathways before assigning a specific coordination number and coordination geometry.

CONCLUSIONS

(1) The following coordination geometry structural pathways are represented in Cu^{2+} oxysalt minerals:
(a) (4 + 2)-distorted octahedral ↔ square-pyramidal;
(b) (4 + 2)-distorted octahedral ↔ square-planar;
(c) square-pyramidal ↔ square-planar.

(2) MO calculations indicate that there are no energy-barriers along the following structural pathways:
(a) (4 + 2)-distorted octahedral ↔ square-pyramidal;
(b) square-pyramidal ↔ square planar;
(c) square-pyramidal ↔ triangular-bipyramidal.

(3) MO calculations indicate a shallow energy-barrier along the structural pathway from (4 + 2)-distorted octahedral to square-planar geometry.

(4) MO calculations give a large energy-barrier along the structural pathway from (4 + 2)-distorted octahedral to triangular-bipyramidal, and no representative examples along this pathway are observed in minerals.

(5) The MO calculations reported here are in good agreement with the range of $Cu^{2+}\phi_n$ coordination geometries observed in minerals. The combination of observed coordination geometries and theoretical calculations shows that Cu^{2+} coordination in oxysalt minerals should be interpreted in terms of structural pathways.

ACKNOWLEDGEMENTS

The Natural Sciences and Engineering Research Council of Canada supported this work in the form of Post-Graduate and Post-Doctoral Fellowships to PCB and Operating and Equipment grants to FCH. The University of Manitoba provided considerable computer resources. Clare Hall, Cambridge, supported this work with a research fellowship to PCB. The manuscript was significantly improved following reviews by Drs. J.K. Burdett and C.W. Burnham, and editorial work by Drs. C.A. Francis and R.F. Martin.

REFERENCES

ARUGA, A. & NAKAI, I. (1985): Structure of Ca-rich agardite, $(Ca_{0.40}Y_{0.31}Fe_{0.09}Ce_{0.06}La_{0.04}Nd_{0.01})Cu_{6.19}[(AsO_4)_{2.42}(HAsO_4)_{0.49}](OH)_{6.38}\cdot 3H_2O$. *Acta Crystallogr.* **C41**, 161-163.

BRUNTON, G. (1973): Refinement of the callaghanite structure. *Am. Mineral.* **58**, 551.

BURDETT, J.K. (1986): *Molecular Shapes*. Wiley, New York, N.Y.

BÜRGI, H.B. & DUNITZ, J.D. (1983): From crystal statics to chemical dynamics. *Acc. Chem. Res.* **16**, 153-161.

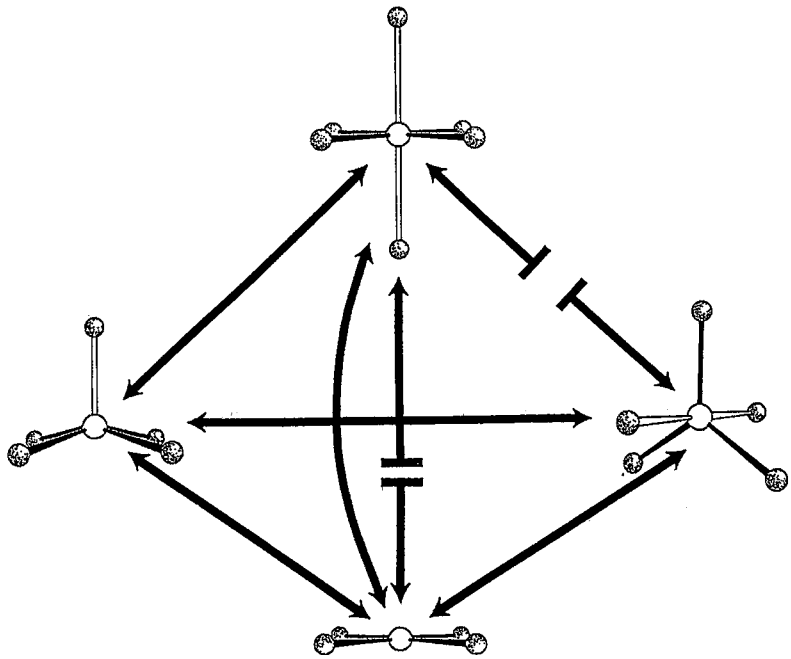

FIG. 12. Structural pathways between $Cu^{2+}\phi_n$ polyhedra as indicated by Hartree–Fock MO calculations. Energy-barriers are represented by breaks in the lines.

CALVO, G. & FAGGIANI, R. (1975): α cupric divanadate. *Acta Crystallogr.* **B31**, 603-605.

COLLINS, J.B., SCHLEYER, P.V.R., BINKLEY, J.S. & POPLE, J.A. (1976): Self-consistent molecular orbital methods. XVII. Geometries and binding energies of second-row molecules. A comparison of three basis sets. *J. Chem. Phys.* **64**, 5142-5151.

CORDSEN, A. (1978): A crystal-structure refinement of libethenite. *Can. Mineral.* **16**, 153-157.

DEETH, R.J. & HITCHMAN, M.A. (1986): Factors influencing Jahn–Teller distortions of six-coordinate copper (II) and low-spin nickel (II) complexes. *Inorg. Chem.* **25**, 1225-1233.

DOBBS, K.D. & HEHRE, W.J. (1987): Molecular orbital theory of the properties of inorganic and organometallic compounds. 5. Extended basis sets for first-row transition metals. *J. Comp. Chem.* **8(6)**, 861-879.

EBY, R.K. & HAWTHORNE, F.C. (1989a): Euchroite, a heteropolyhedral framework structure. *Acta Crystallogr.* **C45**, 1479-1482.

_____ & _____ (1989b): Cornetite: modulated densely-packed Cu^{2+} oxysalt. *Mineral. Petrol.* **40**, 127-136.

_____ & _____ (1990): Clinoclase and the geometry of [5]-coordinate Cu^{2+} in minerals. *Acta Crystallogr.* **C46**, 2291-2294.

_____ & _____ (1993): Structural relations in copper oxysalt minerals. I. Structural hierarchy. *Acta Crystallogr.* **B49**, 28-56.

EFFENBERGER, H. (1977): Verfeinerung der Kristallstruktur von synthetischem Teineit, $CuTeO_3{\cdot}2H_2O$. *Tschermaks Mineral. Petrogr. Mitt.* **24**, 287-298.

_____ (1985): $Cu_2O(SO_4)$, dolerophanite: refinement of the crystal structure, with a comparison of $[OCu(II)_4]$ tetrahedra in inorganic compounds. *Monatsh. Chemie* **116**, 927-931.

_____ (1986): Likasite, $Cu_3(OH)_5(NO_3){\cdot}2H_2O$: revision of the chemical formula and redetermination of the crystal structure. *Neues Jahrb. Mineral. Monatsh.*, 101-110.

_____ (1988): Contributions to the stereochemistry of copper. The transition from a tetragonal pyramidal to a trigonal bipyramidal $Cu(II)O_5$ coordination figure with a structure determination of $PbCu_2(SeO_3)_3$. *J. Solid State Chem.* **73**, 118-126.

EVANS, H.T., JR. & MROSE, M.E. (1977): The crystal chemistry of the hydrous copper silicates, shattuckite and plancheite. *Am. Mineral.* **62**, 491-502.

FANFANI, L., NUNZI, A., ZANAZZI, P.F. & ZANZARI, A.R. (1973): The crystal structure of buttgenbachite. *Mineral. Mag.* **39**, 264-270.

FRISCH, M.J., BINKLEY, J.S., SCHLEGEL, H.B., RAGHAVACHARI, K., MELIUS, C.F., MARTIN, R.L., STEWART, J.J.P., BOBROWICZ, F.W., ROHLFING, C.M., LAHN, L.R., DEFREES, D.J., SEEGER, R., WHITESIDE, R.A., FOX, D.J., FLEUDER, E.M. & POPLE, J.A. (1984): Gaussian 86. Carnegie-Mellon Quantum Chemistry Publishing Unit, Pittsburgh, Pennsylvania.

_____, TRUCKS, G.W., HEAD-GORDON, M., GILL, P.M.W., WONG, M.W., FORESMAN, J.B., JOHNSON, B.G., SCHLEGEL, H.B., ROBB, M.A., REPLOGLE, E.S., GOMPERTS, R., ANDRES, J.L., RAGHAVACHARI, K., BINKLEY, J.S., GONZALEZ, C., MARTIN, R.L., FOX, D.J., DEFREES, D.J., BAKER, J., STEWART, J.J.P. & POPLE, J.A. (1992): Gaussian 92, Revision C, Gaussian Inc., Pittsburgh, Pennsylvania.

GIBBS, G.V. (1982): Molecules as models for bonding in silicates. *Am. Mineral.* **67**, 421-450.

GROAT, L.A. & HAWTHORNE, F.C. (1987): Refinement of the crystal structure of papagoite, $CaCuAlSi_2O_6(OH)_3$. *Mineral. Petrol.* **37**, 89-96.

HATHAWAY, B.J. (1984): A new look at the stereochemistry and electronic properties of complexes of the copper (II) ion. *Structure and Bonding* **57**, 55-118.

HAWTHORNE, F.C. (1985): The crystal structure of stringhamite. *Tschermaks Mineral. Petrogr. Mitt.* **34**, 15-24.

_____ (1986): Lammerite, $Cu_3(AsO_4)_2$, a modulated close-packed structure. *Am. Mineral.* **71**, 206-209.

_____ & GROAT, L.A. (1985): The crystal structure of wroewolfeite, a mineral with $[Cu_4(OH)_6(SO_4)(H_2O)]$ sheets. *Am. Mineral.* **70**, 1050-1055.

HEHRE, W.J., RADON, L., SCHLEYER, P.V.R. & POPLE, J.A. (1986): *Ab initio Molecular Orbital Theory.* John Wiley and Sons, New York, N.Y.

_____, STEWART, R.F. & POPLE, J.A. (1969): Self-consistent molecular-orbital methods. I. Use of gaussian expansions of Slater-type atomic orbitals. *J. Chem. Phys.* **51**, 2657-2664.

HUGHES, J.M. & BROWN, M.A. (1989): The crystal structure of ziesite, β-$Cu_2V_2O_7$, a thortveitite-type structure with a non-linear X–O–X inter-tetrahedral bond. *Neues Jahrb. Mineral. Monatsh.*, 41-47.

_____ & HADIDIACOS, C.G. (1985): Fingerite, $Cu_{11}O_2(VO_4)_6$, a new vanadium sublimate from Izalco volcano, El Salvador: descriptive mineralogy. *Am. Mineral.* **70**, 193-196.

JAHN, H.A. & TELLER, E. (1937): Stability of polyatomic molecules in degenerate electronic states. 1. Orbital degeneracy. *Proc. Roy. Soc., Ser. A* **161**, 220-236.

KELLER, P., HESS, H. & DUNN, P.J. (1979): Die Ladungsbilanz für eine verteinerte Kristallstruktur von Stranskiit, $Zn_2Cu(AsO_4)_2$. *Tschermaks Mineral. Petrogr. Mitt.* **26**, 167-174.

LASAGA, A.C. & GIBBS, G.V. (1987): Applications of quantum mechanical potential surfaces to mineral physics calculations. *Phys. Chem. Minerals* **14**, 107-117.

_____ & _____ (1988): Quantum mechanical potential surfaces and calculations on minerals and molecular clusters. I. STO–3G and 6–31G* results. *Phys. Chem. Minerals* **16**, 29-41.

_____ & _____ (1990): *Ab initio* quantum mechanical calculations of water-rock interactions: adsorption and hydrolysis reactions. *Am. J. Sci.* **290**, 263-295.

_____ & _____ (1991): Quantum mechanical Hartree–Fock potential surfaces and calculations in minerals. II. 6–31G* results. *Phys. Chem. Minerals* **17**, 485-491.

LAUGHON, R.B. (1971): The crystal structure of kinoite. *Am. Mineral.* **56**, 193-200.

LINDQUIST, O. (1972): The crystal structure of $CuTeO_3$. *Acta Chem. Scand.* **26**, 1423-1430.

MCCAMMON, C.A., BROWN, T.H. & MEAGHER, E.P. (1991): Calculation of the equation of state and elastic moduli of MgO using molecular orbital theory. *Phys. Chem. Minerals* **17**, 622-628.

MELLINI, M. & MERLINO, S. (1979): Posnjakite: $^2_\infty[Cu_4(OH)_6(H_2O)O]$ octahedral sheets in its structure. *Z. Kristallogr.* **149**, 249-257.

NAKAI, I. (1986): Henmilite, $Ca_2Cu(OH)_4[B(OH)_4]_2$, a new mineral from Fuka, Okayama Prefecture, Japan. II. Crystal structure. *Am. Mineral.* **71**, 12-40.

NEWTON, M.D. & GIBBS, G.V. (1980): *Ab initio* calculated geometries and charge distributions for H_4SiO_4 and $H_6Si_2O_7$ compared with experimental values for silicates and siloxanes. *Phys. Chem. Minerals* **6**, 221-246.

ORGEL, L.E. (1966): *An Introduction to Transition Metal Chemistry: Ligand-Field Theory* (second ed.). Methuen, London, U.K.

OSWALD, H.R., RELLER, A., SCHMALLE, H.W. & DUBLER, E. (1990): Structure of copper (II) hydroxide, $Cu(OH)_2$. *Acta Crystallogr.* **C46**, 2279-2284.

PASERO, M. & PERCHIAZZI, N. (1989): Chalcomenite from Baccu Locci, Sardinia, Italy: mineral data and structure refinement. *Neues Jahrb. Mineral. Monatsh.*, 551-556.

PIRET, P., DELIENS, M. & PIRET-MEUNIER, J. (1985): Occurrence and crystal structure of kipushite, a new copper–zinc phosphate from Kipushi, Zaire. *Can. Mineral.* **23**, 35-42.

POPLE, J.A. (1976): A priori geometry predictions. *In* Modern Theoretical Chemistry **4** (H.F. Schaefer III, ed.). Plenum Press, New York, N.Y. (1-27).

POZAS, J.M.M., ROSSI, G. & TAZZOLI, V. (1975): Re-examination and crystal structure analysis of litidionite. *Am. Mineral.* **60**, 471-474.

SHANNON, R.D. & CALVO, C. (1972): Crystal structure of a new form of $Cu_3V_2O_8$. *Can. J. Chem.* **50**, 3944-3949.

_____ & _____ (1973): Crystal structure refinement of $Cu_5V_2O_{10}$. *Acta Crystallogr.* **B29**, 1338-1345.

SHOEMAKER, G.L., ANDERSON, J.B. & KOSTINER, E. (1977): Refinement of the crystal structure of pseudomalachite. *Am. Mineral.* **62**, 1042-1048.

STAROVA, G.L., FILATOV, S.K., FUNDAMENSKY, V.S. & VERGASOVA, L.P. (1991): The crystal structure of fedotovite, $K_2Cu_3O(SO_4)_3$. *Mineral. Mag.* **55**, 613-616.

TOMAN, K. (1977): The symmetry and crystal structure of olivenite. *Acta Crystallogr.* **B33**, 2628-2631.

ZIGAN, F. & SCHUSTER, H.D. (1972): Verfeinerung der Struktur von Azurit, $Cu_3(OH)_2(CO_3)_2$, durch Neutronenbeugung. *Z. Kristallogr.* **135**, 416-436.

Received September 13, 1994, revised manuscript accepted February 17, 1995.